Simultaneous Wireless Power and Data Transfer System With Full-Duplex Mode Based on LCC/CLC Resonant Network

Yongzhi Jing, Wei Feng, Ke Qiao, Liangtao Yang, Sen Wang, and Linhai Lu

***Abstract*—Demand for the wireless power transmission system with real-time and full-duplex data transmission, a high-frequency carrier injection full-duplex simultaneous wireless power and data transfer (SWPDT) system is proposed. An *LCC/CLC* compensation structure is applied in the power transfer channel to achieve voltage stabilization and reduce the power interference on the data transmission. An *LC* parallel branch is utilized in the data receiving circuit to suppress ipsilateral data source crosstalk in full-duplex communication. This article theoretically demonstrates the voltage gain characteristics of the power and data transfer channels. Then, the crosstalk between bidirectional data transmission is discussed, along with the analysis of the power effect on the data transmission. In addition, the parameter design method is presented to optimize the data transmission gains while suppressing interference and crosstalk. Finally, the experimental prototype with 20 W output power, 250 kbps forward data rate, and 170 kbps backward data rate is built to verify the correctness and effectiveness of the proposed full-duplex SWPDT system.**

***Index Terms*—Amplitude-shift keying (ASK), full-duplex communication, shared channel transmission, wireless power transfer (WPT).**

I. Introduction

WIRELESS power transfer (WPT) technology can transmit electric energy from a power source to a load without conductors. With years of development, WPT technology has been widely used in electronic devices, smart homes, electric vehicles, industrial robots, and underwater detection equipment [1], [2] [3], [4]. In these applications, real-time communication between the primary and secondary sides is required to improve the overall system performance, such as closed-loop control, instruction exchange, load detection, and state-of-charge monitoring [5], [6]. Therefore, simultaneous wireless power and data transmission (SWPDT) has recently gained more attention.

The SWPDT techniques can be mainly classified into multichannel and single-channel SWPDT [7]. The first type of multichannel SWPDT is to use conventional communication modules, such as Bluetooth, Zigbee, and Wi-Fi, which can achieve high-speed data transmission. However, the complexity and cost of the system are increased, and the delay caused by the pairing time of these modules limits their application. The second type of multichannel SWPDT is to use additional data transmission coils. This way can achieve high-speed bidirectional data transmission. But it also increases system complexity, and the interference between the power and data transmission coils must be considered. The first type of single-channel SWPDT is to modulate the amplitude, frequency or phase of the power wave to characterize the data [8], [9]. This method is simple to implement, but the data transmission rate is limited by the frequency of the power wave and generally only reaches a few kbps. Besides, this method changes the characteristics of the power wave, so the data transmission has a significant impact on power transmission. The second type of single-channel SWPDT is to inject the modulated high-frequency carrier containing the data characteristics into the power wave. The data transmission rate is almost unaffected by power transmission, and the interference between power transmission and data transmission is smaller than the power wave modulation method.

Nowadays, the high-frequency carrier injection SWPDT is attracting wide attention due to its small size, low crosstalk, and high transmission rate. However, the current SWPDT is focused on unidirectional or half-duplex data transmission. Yao et al. [10] show an frequency-shift keying (FSK)-based SWPDT scheme that is less susceptible to interference between the power and data transfer. In [11], the double-D coupling coil is used to transfer power and data simultaneously. The data carriers are directly injected into one of the D coils and can be entirely coupled to the data receiving side. In [12], the power and data can be transferred via the same channel based on the time-division multiplexing theory. In [13], the single-coil and dual-resonant coupling structure are proposed to transmit power and data simultaneously. Sun et al. [14] present a topology that data carriers are injected and extracted in parallel to increase the data transmission gain and achieve half-duplex communication.

Manuscript received 12 August 2022; revised 11 November 2022; accepted 23 November 2022. Date of publication 29 November 2022; date of current version 14 February 2023. This work was supported by the National Natural Science Foundation of China under Grant 52077183. Recommended for publication by Associate Editor A. Kuperman. *(Corresponding author: Yongzhi Jing.)*

Yongzhi Jing, Wei Feng, Ke Qiao, and Sen Wang are with the Key Laboratory of Magnetic Suspension Technology and Maglev Vehicle, Ministry of Education, Southwest Jiaotong University, Chengdu 610031, China, and also with the School of Electrical Engineering, Southwest Jiaotong University, Chengdu 610031, China (e-mail: jingyongzhi@swjtu.edu.cn; feng132@my.swjtu.edu.cn; qiaoke0637@163.com; a1571612293@163.com).

Liangtao Yang and Linhai Lu are with the Tangshan Graduate School of Southwest Jiaotong University, Tangshan 063000, China (e-mail: yangliangtao@my.swjtu.edu.cn; llhai602@163.com).

Color versions of one or more figures in this article are available at https://doi.org/10.1109/TPEL.2022.3225320.

Digital Object Identifier 10.1109/TPEL.2022.3225320

In consideration of the communication efficiency of the SWPDT system, full-duplex data transmission is required. Although the single-channel SWPDT based on data carrier has been developed for years, there are still some problems in the application of full-duplex communication [15], such as crosstalk between bidirectional data transmission and the interference of power transmission. In [16], a topology with a dual-notch filter is used to reduce the interference of ipsilateral data source, but this method needs more passive components. In [17], a full-duplex SWPDT is proposed based on differential quadrature phase-shift keying (DQPSK). The plug-and-play data injector and extractor make the system design simpler than the conventional method. Nevertheless, the data transmission rate is relatively low at 64 kbps. In [18], the data transfer channel is constituted by a four resonance dual-rejection structure, which achieves full-duplex data transmission effectively. However, it requires four sets of wave trappers in the power transfer channel. Wang et al. [19] achieve an improvement of signal-to-noise ratio (SNR) for SWPDT system with double-side *LCCL* compensation topology and dual-resonant structure. However, two blocking inductances are added in the power transfer channel, and the parameters of the data transmitting circuit and receiving circuit are coupled with each other, which leads to a more complex parameter configuration. In summary, the system structure or parameter configuration of the data transfer channel mentioned above is relatively complex, which leads to the system is not easy to implement.

Recently, the double-side *LCC* compensation topology has been widely used in SWPDT systems due to its effectiveness in reducing the effect of power transmission on data transmission [20], which can implement load-independent constant current output, just as most of the existing works. However, the constant voltage output is required in some other applications. The existing constant voltage topologies (e.g., *LCC/S, S/LCC*, etc.) are not suitable for SWPDT because there is a series compensation side, which leads to more interference on the data transmission by the high-frequency component of the power carrier. However, the multi resonant compensation (e.g., *LC, LCC, CLC*, etc.) provides a path for the high-frequency component, thus, the double-side multi resonant topology (e.g., *LCC/CLC*) is more suitable for the constant voltage output SWPDT.

In order to achieve constant voltage output, suppress power interference, and make the system easy to implement, this article presents a new high-frequency carrier injection full-duplex SWPDT system. An *LCC/CLC* multiresonant network is used to effectively achieve voltage stabilization and suppress the power interference on the data transmission in the proposed system. On this basis, an *LC* parallel branch is connected serially to each data receiving circuit to minimize interference between bidirectional data transmission. The rest of this article is organized as follows. Section II presents an overview of the proposed system, including the composition and parameter configuration of the power and data transfer channels. In Section III, the voltage gain is deduced in the power and data transfer channels, respectively. Section IV discusses the main interference in the proposed SWPDT system, and the parameters design is carried out to optimize the data transmission gains and suppress interference. Section V presents the experimental validation results for the theoretical analysis. Finally, Section VI concludes this article.

II. Overview of the Proposed System

The proposed SWPDT system is composed of power and data transfer channels shown in Fig. 1. The power transfer channel consists of the dc power supply, the full-bridge inverter, the *LCC/CLC* compensation topology, loose-coupling coils, the diode rectifier, and the load resistor. The data transfer channel consists of the modulated data source, compensation components, data coupling transformers, loose-coupling coils, the parallel *LC* branch, and receiving resistor. The primary and secondary sides of the proposed SWPDT system each have a data transmitting circuit and a data receiving circuit to achieve data full-duplex transmission. C_1 in the *LCC* network provides a path for the high-frequency component of the power carrier generated by the inverter. Similarly, C_2 in the *CLC* network provides a path for the high-frequency component generated by the rectifier. These high-frequency components hardly pass through the data receiving circuits, and the interference of the power carrier can be effectively suppressed relative to series compensation.

The *LCC* network is utilized at the primary side of the power transfer channel, and the resonant components L_1, C_1, L_p, C_p, L_{dt1} and L_{dr1} should satisfy

$$\omega_p = 1/\sqrt{L_1 C_1} = 1/\sqrt{(L_p + L_{dt1} + L_{dr1} - L_1)\, C_p} \quad (1)$$

where ω_p is the power transfer carrier frequency.

The *CLC* topology is adopted for the secondary side of the power transfer channel. The parameters L_s, L_{dt2}, L_{dr2} and C_s satisfy series resonance, and the parameters L_2 and C_2 satisfy parallel resonance. These resonant parameters should satisfy

$$\omega_p = 1/\sqrt{(L_s + L_{dt2} + L_{dr2})\, C_s} = 1/\sqrt{L_2 C_2}. \quad (2)$$

The parallel capacitors C_1 and C_2 in the *LCC/CLC* resonant network can filter out a large portion of the high-order harmonics generated by the primary inverter circuit and the secondary rectifier circuit. So, there is almost no high-frequency component of the power wave on the receiving resistor for both the primary side and secondary side, which is very advantageous for the data transmission.

The data transfer channel is serially connected with the power transfer channel via the data coupled transformers. The data sources which represent the modulated data are U_{d1} and U_{d2} at the forward and backward data transmissions, respectively. After the series resonant components, U_{d1} and U_{d2} are injected into the power transfer channel by the data coupled transformers T_{dt1} and T_{dt2}. The data carriers can be transmitted to the opposite side through the loose-coupling coils L_p and L_s. Then, they can be extracted by the data coupled transformers T_{dr1} and T_{dr2}. The demodulation circuit can recover the high-frequency analog signal to the corresponding digital signal.

In order to realize full-duplex communication, dual frequencies ω_{d1} and ω_{d2} are selected to transmit forward and backward data separately. The forward and backward data transmission can be analyzed entirely independently. Take the forward data

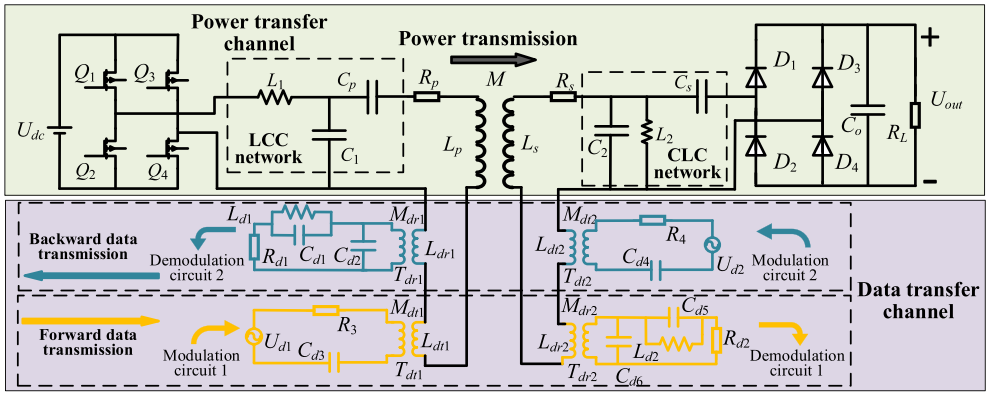

Fig. 1. Structure of proposed SWPDT system with full-duplex communication.

transmission as an example. The resonant frequency of C_{d3} and L_{dt1} in the data transmitting circuit is ω_{d1}. The resistor R_3 is used to regulate dynamic response speed and data transmission power level. In order to avoid crosstalk between the bidirectional data transmission, the *LC* parallel branch is connected in series in the secondary side receiving circuit. The resonant frequency of the *LC* parallel branch L_{d2} and C_{d5} is designed as backward data carrier frequency ω_{d2}. Therefore, the secondary side modulated signal is significantly attenuated in the secondary side receiving circuit, and the interference from the carrier U_{d2} is hardly received on the receiving resistor R_{d2}. To increase the data transmission voltage gain, the C_{d6} is resonant with L_{dr2} at ω_{d1} in the receiving circuit. Above the analysis on the data transfer channel, these parameters should satisfy

$$\begin{cases} \omega_{d1} = 1/\sqrt{L_{dt1}C_{d3}} = 1/\sqrt{L_{dr2}C_{d6}} \\ \omega_{d2} = 1/\sqrt{L_{d2}C_{d5}}. \end{cases} \tag{3}$$

In the backward data transmission, the compensation circuit is entirely symmetrical to the forward data transmission. The resonant frequency of the *LC* parallel branch L_{d1} and C_{d1} is ω_{d1} in the data receiving circuit, which assures the forward transmission data carrier is significantly attenuated in the backward transmission receiving circuit. The resonant frequency of the L_{dt2} and C_{d4} in the data transmitting circuit is ω_{d2}. Then the C_{d2} is resonant with L_{dr1} at ω_{d2}. These parameters should satisfy

$$\begin{cases} \omega_{d2} = 1/\sqrt{L_{dt2}C_{d4}} = 1/\sqrt{L_{dr1}C_{d2}} \\ \omega_{d1} = 1/\sqrt{L_{d1}C_{d1}}. \end{cases} \tag{4}$$

III. Analysis on Transfer Channel

A. Analysis on Power Transfer Channel

When only the power transfer channel is analyzed, the data sources U_{d1} and U_{d2} in the data transfer channel can be treated as short circuits. Due to the *LCC/CLC* compensation structure with good frequency selection characteristics, the fundamental harmonic approximation can be applied here. The high-order harmonics generated by the dc full-bridge inverter are not considered, and the power supply is treated as an ideal ac source. The RMS value of the fundamental component of the inverter voltage is expressed as $U_{\text{in}} = 2\sqrt{2}U_{\text{dc}}/\pi$. The AC equivalent resistance R_E is given by

$$R_E = 8R_L/\pi^2 \tag{5}$$

where R_L is the dc load resistance.

At the primary side of the proposed SWPDT system, the impedances of data transmitting and receiving circuits in the data transfer channel are Z'_{dt1} and Z'_{dr1}, respectively, and the impedances are calculated by

$$\begin{cases} Z'_{dt1} = j\omega_p L_{dt1} + 1/j\omega_p C_{dt3} + R_3 \\ Z'_{dr1} = j\omega_p L_{dr1} + (1/j\omega_p C_{d2}) \,//\, \left[R_{d1} + \frac{j\omega_p L_{d1}}{1-\omega_p^2 L_{d1}C_{d1}}\right]. \end{cases} \tag{6}$$

The corresponding equivalent impedances in the power transfer channel are Z_{dt1} and Z_{dr1}, respectively, and the impedances are obtained as

$$\begin{cases} Z_{dt1} = (\omega_p M_{dt1})^2 / Z'_{dt1} \\ Z_{dr1} = (\omega_p M_{dr1})^2 / Z'_{dr1} \end{cases} \tag{7}$$

where M_{dt1} and M_{dr1} are the mutual inductances of the data coupled transformers T_{dt1} and T_{dr1}, respectively.

Generally, the ω_p is much lower than data carrier frequencies ω_{d1} and ω_{d2}. From (6), it can be seen that the impedances Z'_{dt1} and Z'_{dr1} are at high-impedance state. So Z_{dt1} and Z_{dr1} can be neglected because they are at low-impedance state and reach close to zero.

At the secondary side of the system, similarly, the equivalent impedances of data transmitting and receiving circuits in the power transfer channel are Z_{dt2} and Z_{dr2}, which can also be neglected. The equivalent circuit of the power transfer channel is shown in Fig. 2.

From (1) and (2), the secondary side impedance $Z_s = R_E + R_s$, and the primary side impedance Z_p can be obtained as

$$Z_p = (\omega_p L_1)^2 / (R_p + Z_{sp}) \tag{8}$$

where the equivalent impedance $Z_{sp} = (\omega_p M)^2 / Z_s$, M is the mutual inductance of the loose-coupling coils, and R_p and R_s are the internal resistance of L_p and L_s.

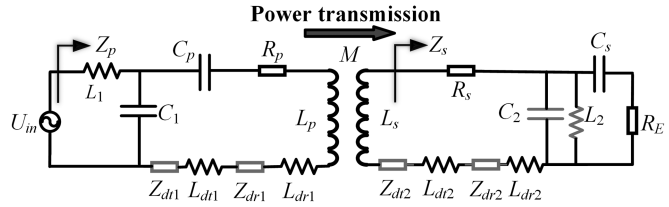

Fig. 2. Equivalent circuit of the power transfer channel.

So, the currents of the primary and secondary side coils are I_p and I_s, respectively, and they can be expressed as

$$\begin{cases} I_p = \frac{U_{\text{in}}}{Z_p} \frac{1}{j\omega_p C_1} \frac{1}{Z_{sp}+R_p} \\ I_s = j\omega_p M I_p / Z_s. \end{cases} . \tag{9}$$

According to (8) and (9), the output voltage across the equivalent ac resistance is found to be

$$U_o = \frac{MU_{\text{in}}}{L_1} \frac{R_E}{R_E + R_s} \approx \frac{MU_{\text{in}}}{L_1}. \tag{10}$$

From (10), when the internal resistance R_s is ignored, the voltage gain is only related to the ratio of M and L_1. If the mutual inductance M is constant, the output voltage U_o can be changed by shifting the L_1. The output power P_o can be expressed as

$$P_o = U_o^2 / R_E. \tag{11}$$

According to the above analysis of the power transfer channel, the power transfer efficiency of the proposed SWPDT system can be expressed as

$$\eta = \frac{\left(\omega_p M L_1\right)^2 R_E}{L_1^2 (R_E + R_s)^2 (R_p + Z_{sp})}. \tag{12}$$

B. Analysis on Data Transfer Channel

When only the data transfer channel is analyzed, the power supply U_{dc} in the power transfer channel can be treated as a short-circuit. At the data carrier frequencies ω_{d1} and ω_{d2}, the capacitors in the power transfer channel are at low-impedance state, and the inductors are at high-impedance state. Take the forward data transmission as an example to derive the transfer function of data transmission. The modulated signal is injected from the data carrier source U_{d1} and extracted across the receiving resistor R_{d2}. The equivalent circuit of the data transfer channel is shown in Fig. 3.

The impedances of each part can be obtained as

$$\begin{cases} Z_{df1} = -(sM_{dt1})^2 / Z_{df2} + 1/sC_{d3} + sL_{dt1} + R_3 \\ Z_{df2} = -(sM)^2 / Z_{df3} + s\left(L_p + L_{dr1} + L_{dt1}\right) \\ \quad + Z_{dr1} + R_p + 1/sC_p + sL_1 // \left(1/sC_1\right) \\ Z_{df3} = -(sM_{dr2})^2 / Z_{df4} + s\left(L_{dt2} + L_{dr2} + L_s\right) \\ \quad + Z_{dt2} + R_s + \left(R_E + 1/sC_s\right) // sL_{d2} // \left(1/sC_2\right) \\ Z_{df4} = \left(R_{d2} + sL_{d2} // \left(1/sC_{d5}\right)\right) // \left(1/sC_{d6}\right) + sL_{dr2} \end{cases} \tag{13}$$

where Z_{dr1} is the equivalent impedance of the data receiving circuit in the primary side, and Z_{dt2} is the equivalent impedance

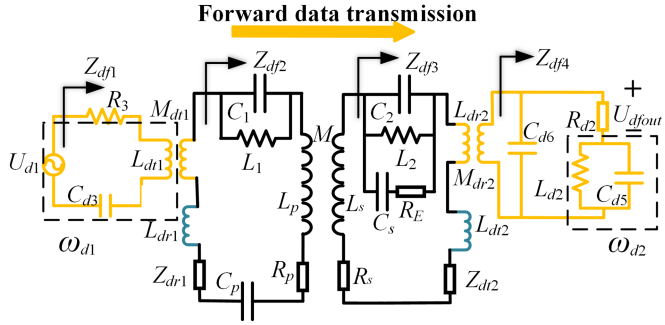

Fig. 3. Equivalent circuit of the forward data transfer channel.

of the data transmitting circuit in the secondary side. They can be calculated as follows:

$$\begin{cases} Z_{dr1} = \frac{-(sM_{dr1})^2}{(R_{d1}+sL_{d1}//(1/sC_{d1}))//(1/sC_{d2})+sL_{dr1}} \\ Z_{dt2} = \frac{-(sM_{dt2})^2}{(1/sC_{d4})+sL_{dt2}+R_4}. \end{cases} \tag{14}$$

According to the above analysis, the transfer functions of each part in the forward data transmission can be obtained as

$$\begin{cases} G_{df1} = 1/Z_{df1} \\ G_{df2} = sM_{dt1} \\ G_{df3} = 1/Z_{df2} \\ G_{df4} = sM \\ G_{df5} = 1/Z_{df3} \end{cases} \begin{cases} G_{df6} = sM_{dr2} \\ G_{df7} = 1/Z_{df4} \\ G_{df8} = \frac{(1/sC_{d6})R_{d2}}{1/sC_{d6}+(1/sC_{d5})//sL_{d2}+R_{d2}}. \end{cases} \tag{15}$$

Based on (15), the transfer function G_{df} at forward data transmission can be obtained as

$$G_{df} = U_{df\text{out}}/U_{d1} = \prod_{i=1,2,3,4,5,6,7,8} G_{df\,i} \tag{16}$$

where $U_{df\text{out}}$ is the output voltage across the receiving resistance R_{d2}. It should be noticed that the gain G_{df} is calculated at the forward data carrier frequency ω_{d1}.

According to (13)–(16), it can be seen that the data transmission voltage gain is dependent on almost the entire system parameters, of which the loose-coupling coils, the data coupled transformers, and the resistors in the data transfer channel are the most significant parts. The self- and mutual-inductance of the loose-coupling coils are generally determined by the power transmission characteristics.

In the design of the system parameters, in order to simplify the analysis and maintain symmetry of forward and backward transfer, assuming that the inductances and coupling coefficients of two transmitting transformers and two receiving transformers are identical, respectively,

$$\begin{cases} L_{dt1} = L_{dt2} = L_{dt} \\ k_{dt1} = k_{dt2} = k_{dt} \end{cases} \begin{cases} L_{dr1} = L_{dr2} = L_{dr} \\ k_{dr1} = k_{dr2} = k_{dr}. \end{cases} \tag{17}$$

The relationship between data transmission gain G_{df} and inductance L_{dt} and L_{dr} is shown in Fig. 4. As the increase of L_{dt}, the gain tends to increase firstly, and the maximum gain occurs at about $L_{dt} = 3$ μH. The gain keeps growing with the rise of L_{dr}, but the effect is not very noticeable. The relationship between data transmission gain and capacitance C_{d3} and C_{d6}

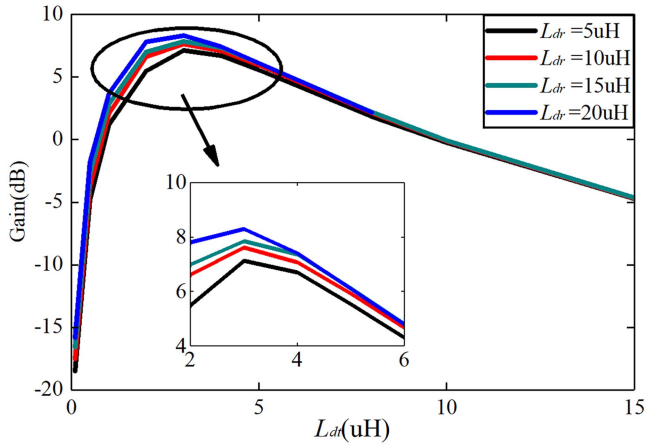

Fig. 4. Forward data transmission gain versus L_{dt}, L_{dr}.

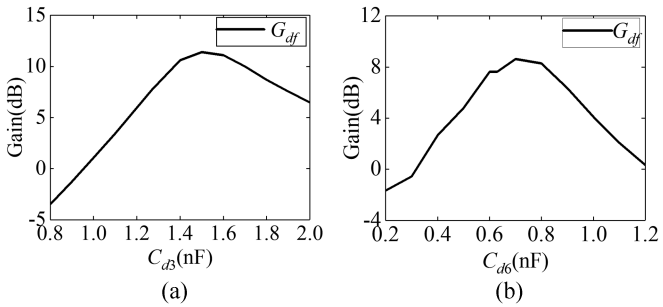

Fig. 5. Forward data transmission gain versus (a) C_{d3} and (b) C_{d6}.

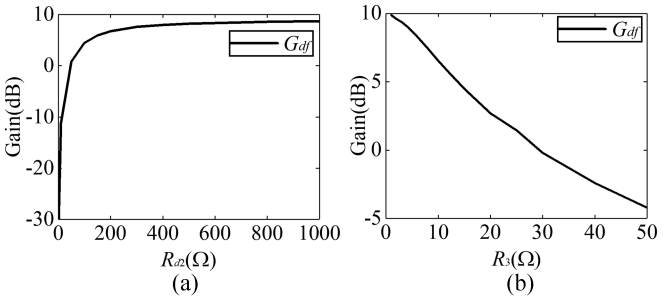

Fig. 6. Forward data transmission gain versus (a) R_{d2} and (b) R_3.

is depicted in Fig. 5. As approaching the designed value of the C_{d3} and C_{d6}, the data transmission gain is maximal, while the data transmission gain decreases sharply as the set values of the C_{d3} and C_{d6} deviate.

The relationship between data transmission gain and R_{d2} and R_3 is shown in Fig. 6. The transmission gain increases with the increase of R_{d2}. When R_{d2} is at a relatively large value, the transmission gain is almost unchanging. Obviously, the larger the value of R_3, the smaller the data transmission gain. But the R_3 is also related with the dynamic performance of the proposed SWPDT system. For amplitude-shift keying (ASK) modulation, the small R_3 increase the transient time, and thus limit the data rate [21]. So R_3 should be considered

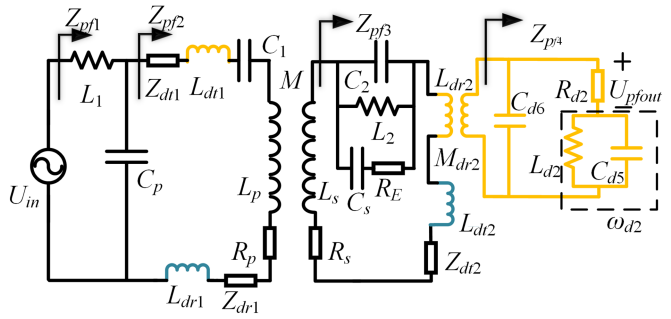

Fig. 7. Equivalent circuit to calculate power interference on forward data transmission.

comprehensively to fulfill the optimal data transmission gain and rate.

The backward data transfer function G_{db} can be obtained in the same way as the forward data transmission and will not be described here. It should be noted that the gain G_{db} is calculated at the backward data carrier frequency ω_{d2}.

IV. Interference Analysis

There are mainly three parts of interference in the proposed full-duplex SWPDT: interference of data transmission on power transmission; interference of power transmission on data transmission; and crosstalk between the forward and backward data transmission.

A. Interference of the Data Transfer on the Power Transfer

Two aspects need to be considered when analyzing the impact of data transmission on power transmission, namely the additional data transmission channels and data transmission carriers. On the one hand, the power current will generate some power loss in the data reception resistors, but this value is quite small. On the other hand, since the data transmission frequency is much larger than the power transmission frequency, the amplitudes of the data carriers are severely attenuated because of the resonant circuits in the power transfer channel. It is much smaller than the power transmission carrier amplitude. Therefore, the impact of data transmission on power transmission is small enough to be generally neglected.

B. Interference of the Power Transfer on the Data Transfer

In order to achieve high-quality data transfer, the interference of power transfer should be minimized as possible. The power transmission interference on the forward data transmission is taken as an example to demonstrate the effect of the power transfer channel. The equivalent circuit is shown in Fig. 7 to calculate the power interference transfer function G_{pf}.

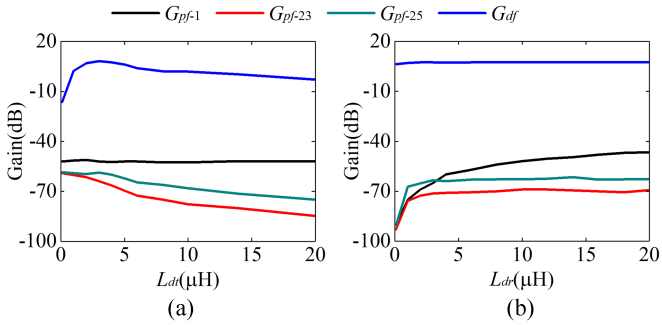

Fig. 8. $G_{pf\text{-}1}$, $G_{pf\text{-}23}$, $G_{pf\text{-}25}$, and G_{df} versus (a) L_{dt} and (b) L_{dr}.

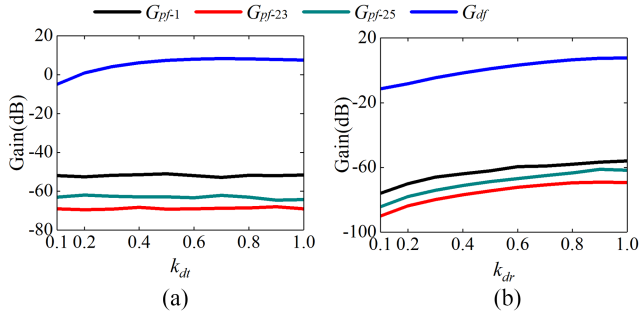

Fig. 9. $G_{pf\text{-}1}$, $G_{pf\text{-}23}$, $G_{pf\text{-}25}$, and G_{df} versus (a) k_{dt} and (b) k_{dr}.

The calculation method is similar to the data transfer function G_{df}. The impedances of each part can be expressed as

$$\begin{cases} Z_{pf1} = (1/sC_p)\,//\,Z_{pf2} + sL_1 \\ Z_{pf2} = \frac{-s^2M^2}{Z_{pf3}} + Z_{dr1} + Z_{dt1} \\ \qquad\quad +s\left(L_p + L_{dr1} + L_{dt1}\right) + R_p + 1/sC_1 \\ Z_{pf3} = Z_{df3} \\ Z_{pf4} = Z_{df4} \end{cases} \tag{18}$$

where $Z_{dt1} = -(sM_{dt1})^2/(R_3 + sL_{dt1} + 1/sC_{d3})$. The transfer functions of each part can be expressed as

$$\begin{cases} G_{pf1} = 1/Z_{pf1} \\ G_{pf2} = 1/(1 + sC_pZ_{pf2}) \\ G_{pf3} = sM \end{cases} \quad \begin{cases} G_{pf4} = 1/Z_{pf3} \\ G_{pf5} = sM_{dr2} \\ G_{pf6} = 1/Z_{pf4} \\ G_{pf7} = G_{df8}. \end{cases} \tag{19}$$

Therefore, the power interference transfer function G_{pf} at forward data transmission can be expressed as

$$G_{pf} = U_{pf\text{out}}/U_{\text{in}} = \prod_{i=1,2,3,4,5,6,7} G_{pfi} \tag{20}$$

where $U_{pf\text{out}}$ is the power interference output voltage across the receiving resistor.

The square wave power supply generated by the inverter circuit contains fundamental and high-order harmonics. Only the fundamental harmonic and the two high-order harmonics closest to the data carrier frequency need to be analyzed. The forward data transmission carrier frequency f_{d1} is 2 MHz, and the nearest 23rd and 25th harmonics frequencies are 1.92 and 2.13 MHz, respectively.

The gain G_{pf} at a frequency of $\gamma \times \omega_p$ is denoted as $G_{pf\text{-}\gamma}$ ($\gamma = 1$, 23 and 25). Each interference gain under different L_{dt} and L_{dr} is shown in Fig. 8. The data transmission gain is also added in Fig. 8, and the difference between the data transmission and interference gains can be understood as the SNR. From Fig. 8(a), the fundamental harmonic of the power wave is almost unchanged, about -52 dB, and the high-order harmonics show a slightly decreasing trend. From Fig. 8(b), as the increase of L_{dr}, the interference gain gradually increases but remains in a relatively small range. It should be noted that the overall amplitude of power-to-data transmission interference is quite small, about -50 dB and below, which proves the superiority of the *LCC/CLC* topology.

The coupling coefficients of the data coupled transformers are also the key factors in improving the SNR. The relationship between transmission gains and coupling coefficients k_{dt} and k_{dr} is shown in Fig. 9. From Fig. 9(a), the three power interference curves almost have not changed, and k_{dt} could be shifted to increase the SNR. From Fig. 9(b), the SNR basically does not change with the growth of k_{dr} in the four graphs. Therefore, the larger coupling coefficients in the data transfer channel can be selected for higher SNR and transmission gain.

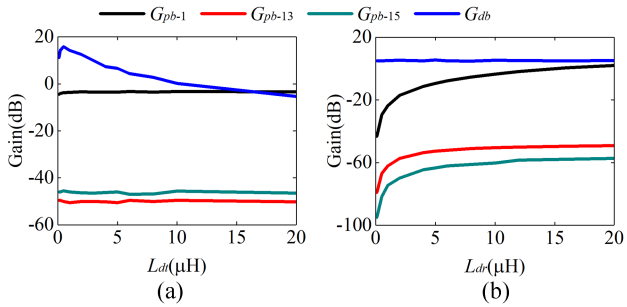

Fig. 10. $G_{pb\text{-}1}$, $G_{pb\text{-}13}$, $G_{pb\text{-}15}$, and G_{db} versus (a) L_{dt} and (b) L_{dr}.

The backward data transmission gain G_{db} and power interference gain G_{pb} can be obtained by the same method as the forward data transmission. The backward data transmission carrier frequency f_{d2} is 1.2 MHz, and the nearest 13th (1.1 MHz) and 15th (1.275 MHz) harmonics in the power carrier need to be analyzed. The gain calculated for G_{pb} at a frequency of $\gamma \times \omega_p$ is denoted as $G_{pb\text{-}\gamma}$ ($\gamma = 1$, 13, and 15). The relationship between transmission gains and L_{dt} and L_{dr} is shown in Fig. 10. As L_{dt} increases, each interference gain is almost constant. However, as L_{dr} increases, each interference gain is in an upward trend, and a smaller value of L_{dr} should be used to avoid too large $G_{pb\text{-}1}$. It should be noted that the $G_{pb\text{-}1}$ is more significant than $G_{pf\text{-}1}$. This is because the backward receiving resistor R_{d1} is on the same side as the power supply, and the fundamental harmonic of the power carrier directly flows to the R_{d1} without passing through the loose-coupling coils in the backward data transmission. Fig. 11 shows the relationship between the backward data transmission and interference gain versus coupling coefficients k_{dt} and k_{dr}. It

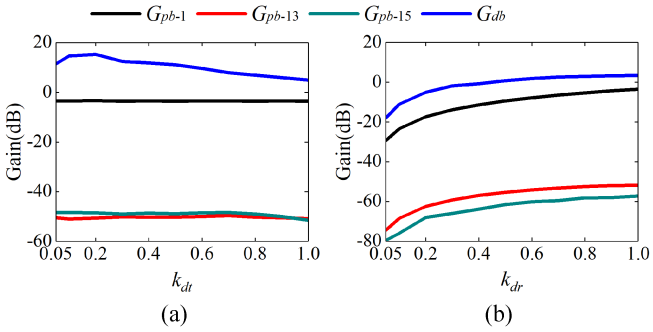

Fig. 11. $G_{pb\text{-}1}$, $G_{pb\text{-}13}$, $G_{pb\text{-}b5}$, and G_{db} versus (a) k_{dt} and (b) k_{dr}.

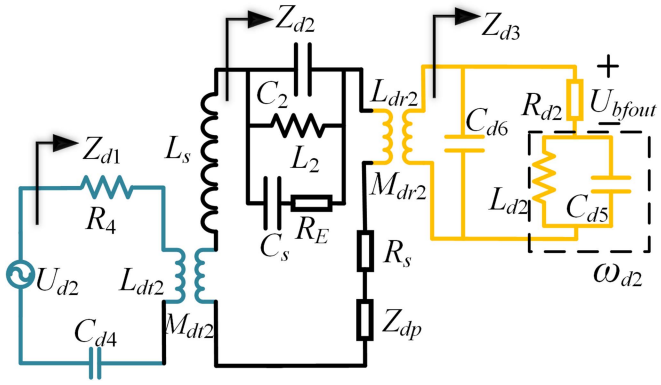

Fig. 12. Equivalent circuit of interference of ipsilateral data source.

is basically the same as the forward data transmission, and k_{dt} and k_{dr} have a weak relationship with SNR.

C. Crosstalk Between Bidirectional Data Transmission

Except for the power interference on the data transfer channel, there is still the interference of the ipsilateral data source. Take the forward data transmission as an example to demonstrate the interference of the backward data source on forward data transmission. The equivalent circuit of interference of the ipsilateral data source is shown in Fig. 12 to calculate the transfer function G_{bf}.

The impedance of each part can be expressed as

$$\begin{cases} Z_{d1} = -(sM_{dt2})^2/Z_{d2} + R_4 + sL_{dt2} + 1/sC_{d4} \\ Z_{d2} = Z_{dp} + s\left(L_s + L_{dr2} + L_{dt2}\right) \\ \quad +R_s - (sM_{dr2})^2/Z_{d3} \\ \quad +\left(R_E + 1/sC_s\right)//sL_2//\left(1/sC_2\right) \\ Z_{d3} = Z_{df4} \end{cases} \tag{21}$$

where Z_{dp} is the equivalent impedance from the primary side circuit to the secondary side and can be calculated as follows equation (22) shown at the bottom of this page:

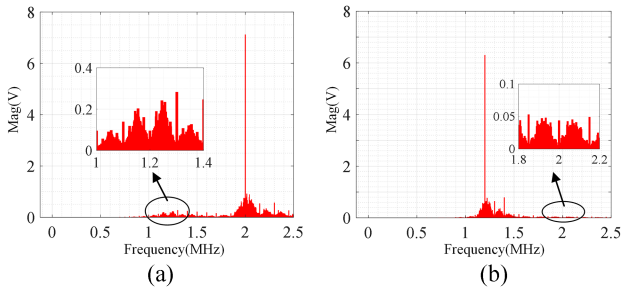

Fig. 13. FFT results. (a) Forward data transmission. (b) Backward data transmission.

The transfer functions of each part can be expressed as

$$\begin{cases} G_{bf1} = 1/Z_{d1} \\ G_{bf2} = sM_{dt2} \\ G_{bf3} = 1/Z_{d2} \end{cases} \quad \begin{cases} G_{bf4} = sM_{dr2} \\ G_{bf5} = 1/Z_{d3} \\ G_{bf6} = G_{df8}. \end{cases} \tag{23}$$

The transfer function G_{bf} of interference of ipsilateral data source can be expressed as

$$G_{bf} = U_{bf\text{out}}/U_{d2} = \prod_{i=1,2,3,4,5,6} G_{bfi} \tag{24}$$

where $U_{bf\text{out}}$ is the output voltage across the receiving resistor R_{d2}. The frequency of ipsilateral data source interference is around ω_{d2} at forward data transmission.

The calculation method of the interference transfer function G_{fb} at backward data transmission is the same as that at forward data transmission. The fast Fourier transform (FFT) results of the data transmission are shown in Fig. 13. From Fig. 13(a), in the forward data transmission, the amplitude of the 2M signal carrier used for the forward transmission is significantly large, while the 1.2 MHz backward data carrier is suppressed. From Fig. 13(b), in the backward transmission, the 2 MHz forward data carrier is suppressed. It is shown that the interference of the ipsilateral data source is even more minor in the backward data transmission and reaches close to zero, and the proposed LC parallel branch can effectively eliminate interference from the ipsilateral data source.

D. Parameters Design Method

Fig. 14 is the flowchart describing the design procedure of the parameters in the proposed full-duplex SWPDT system. First, coil size and transmission distance are confirmed according to the practical application, i.e., the values of L_p, L_s, and M are determined. Then, the frequency of power transfer and data carriers should be selected. After confirming the self-inductance of the data coupled transformer, the power transfer channel parameters L_1, C_1, C_p and C_s can be calculated according to (1) and (2). At the same time, the parameters L_2 and C_2 can be calculated according to (2). The inductance L_1 can be shifted to

$$Z_{dp} = \frac{-(sM)^2}{s\left(L_p + L_{dr1} + L_{dt1}\right) + \frac{1}{sC_p} + R_p + \frac{1}{sC_1}//sL_1 - \frac{(sM_{dt1})^2}{Z_{dt1}} - \frac{(sM_{dr1})^2}{Z_{dr1}}}. \tag{22}$$

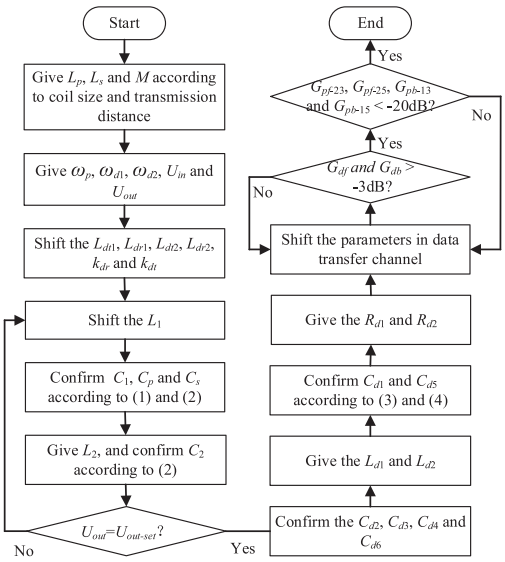

Fig. 14. Flowchart of system parameters design.

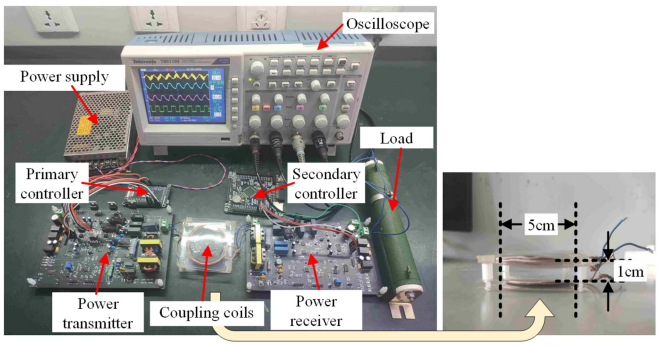

Fig. 15. Experimental platform.

fulfill the rated voltage $U_{\text{out-set}}$ if there is a slight offset in the output voltage.

Since the power transfer channel parameters are confirmed, C_{d2}, C_{d3}, C_{d4}, and C_{d6} are calculated according to (3) and (4). Then, the parameter values of the LC parallel branch and the receiving resistance can be determined. For stable data transmission, the data transmission gain should be greater than -3 dB (receiving voltage amplitude of about 5 V), and power high-frequency interference gain $G_{pf\text{-}23}$, $G_{pf\text{-}25}$, $G_{pb\text{-}13}$, and $G_{pb\text{-}15}$ should be suppressed below -20 dB. At last, the parameters of the entire data channel could be shifted to optimize the data transmission gains while suppressing interference and crosstalk.

V. Experimental Verification

To verify the correctness and effectiveness of the proposed full-duplex SWPDT system, a 20 W prototype is built, as shown in Fig. 15. The specific parameters utilized in the prototype are given in Table I. The proposed SWPDT system is mounted on two PCBs (one for the transmitter and one for the receiver). The size of the coupling coils is 5 cm $\times$ 5 cm, and the transmission

TABLE I
System Parameters

Parameter	Value	Parameter	Value	Parameter	Value
R_L/Ω	29	L_{dt1}, L_{dt2}/μH	5	k_{dt1}, k_{dt2}	0.99
L_p, L_s/μH	29.7	L_{dr1}, L_{dr2}/μH	7.5	k_{dr1}, k_{dr2}	0.99
M/μH	14.5	C_{d1}/nF	0.288	R_{d1}, R_{d2}/Ω	1000
L_1/μH	15	C_{d2}/nF	2.35	U_{dc}/V	24
C_1/nF	242	C_{d3}/nF	1.27	R_3/Ω	6
C_p/nF	125	C_{d4}/nF	3.52	R_4/Ω	3
L_2/μH	15	C_{d5}/nF	0.8	f_p/kHz	85
C_2/nF	233	C_{d6}/nF	0.85	f_{d1}/MHz	2
C_s/nF	82	L_{d1}, L_{d2}/μH	22	f_{d2}/MHz	1.2
Q_1-Q_4	IRFZ24	D_1-D_4	TSSA3U60	-	-

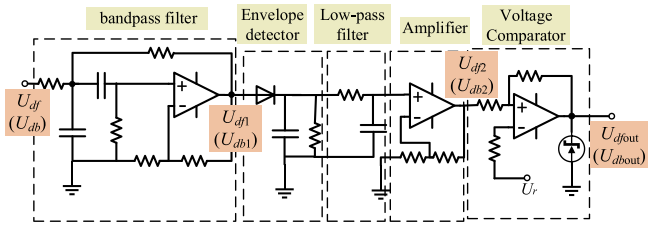

Fig. 16. Demodulation circuit.

distance is 1cm, which is probably applicable to implantable medical equipment, smart home appliances, and mobile devices.

The data modulation scheme is ON-OFF keying and can be regarded as a particular case of ASK. When the digital signal to be transmitted is "1," the 2 MHz or 1.2 MHz data carrier is generated by the half-bridge inverter circuits in the data transfer channel. When the digital signal to be transmitted is "0," shutting down the half-bridge inverter circuits, and there is no high-frequency carrier generation. The demodulation circuit is shown in Fig. 16, which is mainly made up of a bandpass filter, an envelope detector, a low-pass filter, an amplifier, and a voltage comparator. In the forward data transmission, the voltage across the receiving resistor, bandpass filter output voltage, comparator input voltage, and demodulation output voltage are denoted as U_{df}, U_{df1}, U_{df2}, and $U_{df\text{out}}$, respectively. Similarly, these voltages in the backward data transmission are represented as U_{db}, U_{db1}, U_{db2}, and $U_{db\text{out}}$, respectively.

The waveforms of the power transfer channel are shown in Fig. 17. The mean value of the output voltage U_{out} is about 24 V when the load is 29 Ω, so the output power is about 20 W. The curves of output voltage U_{out} and efficiency η under different R_L are shown in Fig. 18. It can be seen that the output voltage shows a slightly increasing trend when the load resistance increases. On the contrary, when the load resistance decreases, the output power increases rapidly and the output voltage drops relatively quickly. When the output power P_o is 20 W, the efficiency is about 80%, and the maximum efficiency is about 82%. The system efficiency is relatively low due to the loss caused by the rectifier circuit and the internal resistances of coupling coils in this low power transfer system. The output power changes from 10 to 30 W by adjusting the load resistance, and the output

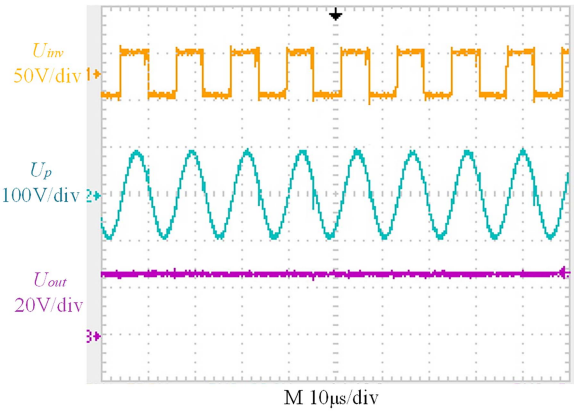

Fig. 17. Waveforms of the power transfer channel: Inverter output voltage $U_{\rm inv}$, the voltage of primary coil U_p, and output voltage $U_{\rm out}$.

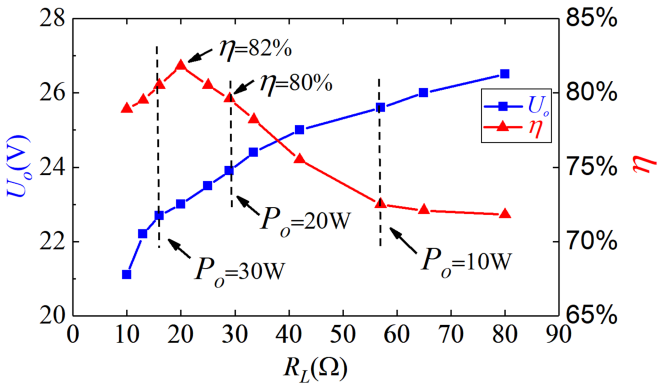

Fig. 18. Output voltage and efficiency under various R_L.

voltage fluctuates within ±6% of the rated voltage. As can be seen, the stabilization of the output voltage within a specific range during load changes is basically achieved.

The forward data transmission rate is set to 250 kbps, and the sequence "10101010" is taken as a binary data example to send. The backward data transmission rate is set to 170 kbps, while taking "10100110" as a data example to send. To better observe the suppression effect of the *LC* parallel branch on interference from the ipsilateral data source, the relevant waveforms without power transmission are shown in Fig. 19. The U_{Ldr1} and U_{Ldr2} are the voltages of the data receiver transformers. The voltages U_{db} and U_{df} across the receiving resistors contain only the data characteristics of the other side to be received. It is evident that the *LC* parallel branch plays a good role in suppressing the ipsilateral data source features.

The critical waveforms in the forward and backward data transmission demodulation circuits with power transmission are shown in Fig. 20. First, the main interference component in the U_{df} and U_{db} is the fundamental harmonic of the power carrier. Second, the high-frequency modulated waves U_{df1} and U_{db1} containing the characteristics of the transmitted data can be well separated by the bandpass filters. Then the envelopes U_{df2} and U_{db2} of the modulated waves are extracted by the envelope detector modules. Finally, the signal envelopes are shaped by

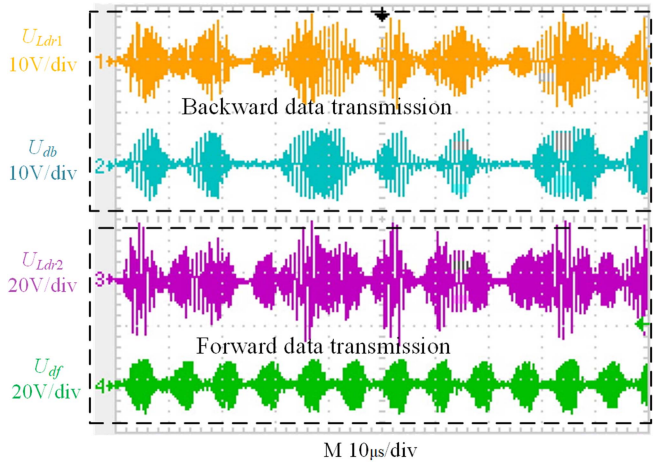

Fig. 19. Voltage waveforms of receiving transformer and receiving resistor without power transmission.

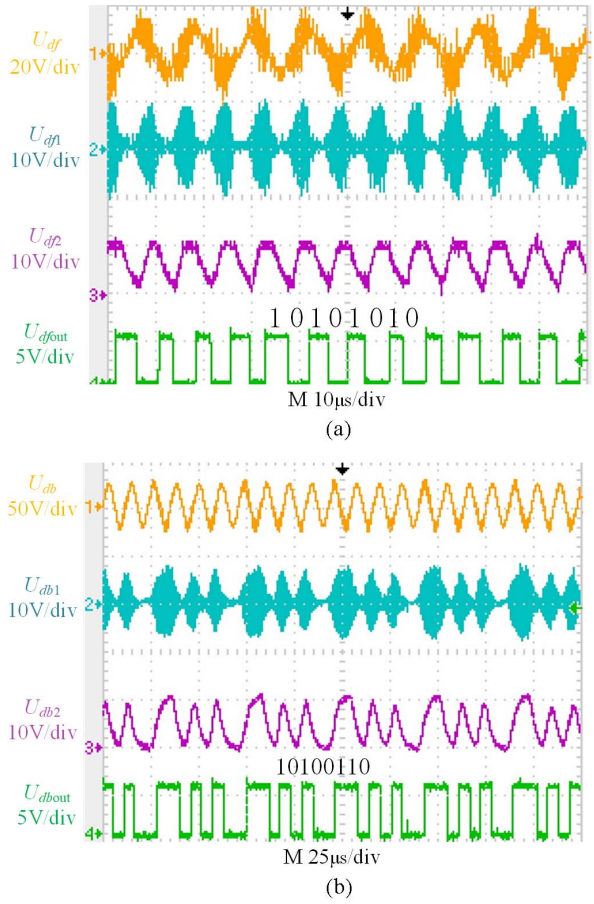

Fig. 20. Demodulate waveforms. (a) Forward data transmission. (b) Backward data transmission.

voltage comparators to recover the transmitted digital signal accurately. In addition, the power loss on the data receiving resistor is about 0.2W, which is 1% or less of the output power, and increasing the data receiving resistor could reduce the loss.

In order to compare and analyze the data transmission characteristics with power transmission and without power transmission, the voltage waveforms of the primary and secondary

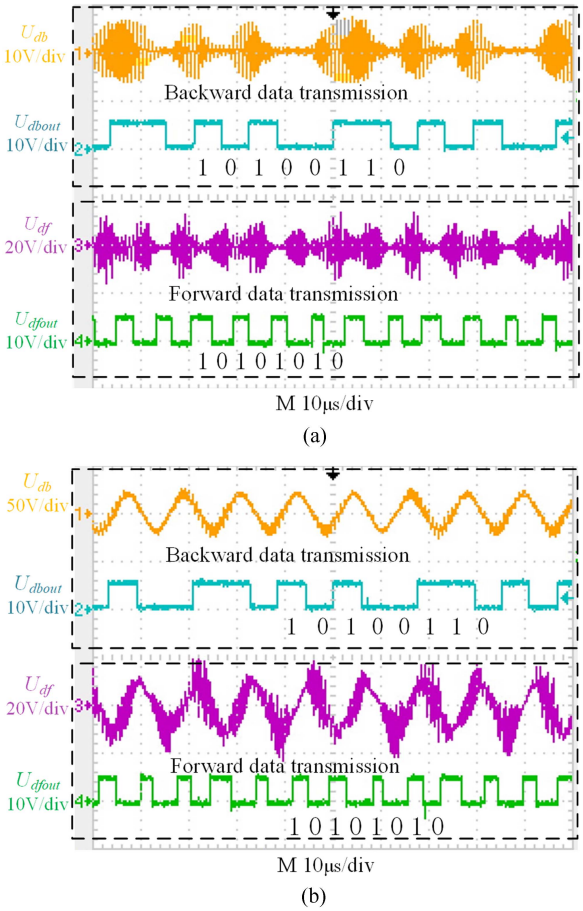

Fig. 21 Waveforms of data transmission. (a) Without power transmission. (b) With power transmission.

TABLE II
BITS ERROR RATE

	Data rate / kbps	P_o / W			
		0	10	20	30
Forward data transmission	128	0	0.086%	0.139%	0.123%
	200	0	0.066%	0.167%	0.172%
	256	0.157%	0.161%	0.290%	0.437%
Backward data transmission	128	0	0.056%	0.182%	0.229%
	170	0	0.122%	0.280%	0.346%

side receiving resistors and the demodulated data are shown in Fig. 21. The received voltage waveforms without power transmission can be better demodulated. When there is power transmission, the received voltage contains both the power carrier and data carrier. However, whether there is power transmission or not, the data can be accurately recovered after the *LC* parallel branch and demodulation circuit. The transmitting and receiving data waveforms are shown in Fig. 22 to analyze the data transmission delay characteristics. It is shown in Fig. 22 that the delay for both the forward and backward data transmission is pretty small, only about 5 μs.

The bit-error-rate (BER) test results of the proposed SWPDT system are given in Table II to verify the accuracy and reliability of data transmission under various operating conditions. Obviously, the higher the transmission rate or energy transmission

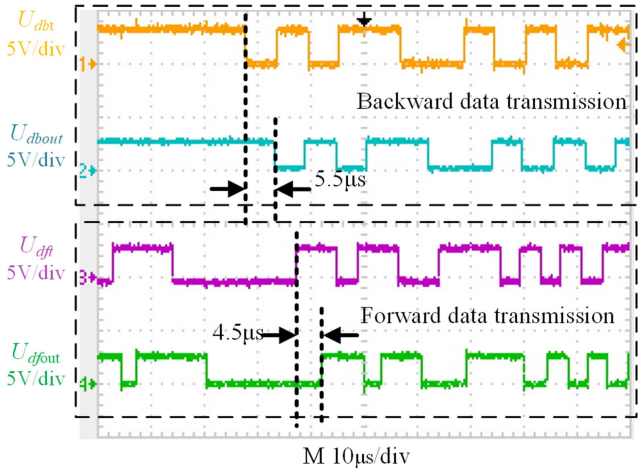

Fig. 22. Waveforms of transmitting data and receiving data.

TABLE III
PERFORMANCE COMPARISON

	This article	[16]	[17]	[18]	[19]
P_o / W	20	400	3300	600	500
Modulation	ASK	ASK	DQPSK	ASK	ASK
Coils size / cm	5*5	40*40	-	-	40*40
Transfer distance / cm	1	30	-	-	30
Data rate / kbps (Forward / Backward)	250 / 170	100 / 200	64 / 64	80 / 80	200 / 600
Number of passive components in the data transfer channel	12	20	14	10	12
The ratio of the carrier frequency to the transmission rate (Forward / Backward)	8 / 7	14 / 21	78 / 97	25 / 15	9.5 / 5.3

power, the higher BER. However, the BER remains at a low level of around 0.3%. The comparison between some typical full-duplex SWPDT references is given in Table III. Compared with other references, the proposed SWPDT system can achieve full-duplex communication with fewer passive components in the data transfer channel. The ratio of the carrier frequency to the transmission rate is comparatively low, which corresponds to a higher transmission rate at the same data carrier frequency. In particular, compared with the typical literature of high power transmission [17], the main advantage of this article is that modulation and demodulation are easier to implement and the data transmission rate is higher. Compared with the typical literature of high data transmission rate [19], the proposed method does not need the blocking inductances in the power transfer channel in this article, and the data transmitting circuit and receiving circuit are designed independently, so the parameter configuration is simpler.

VI. CONCLUSION

In this article, a full-duplex SWPDT system is proposed based on the *LCC/CLC* compensation topology in the power transfer channel and the *LC* parallel branch in the data transfer channel. The *LCC/CLC* network is used to suppress the

interference of power transmission on data transmission and achieve load-independent voltage stabilization. The *LC* parallel branch is connected in series in the data receiving circuit, effectively reducing crosstalk between bidirectional data transmission. The equivalent circuits of the power and data transfer channels are analyzed. The main three parts of interference in the proposed full-duplex SWPDT system are analyzed, and the parameters design is carried out to optimize the data transmission gains and suppress interference. At last, the experimental platform is built to achieve full-duplex communication at 250 kbps forward and 170 kbps backward transmission rates under the 20 W output power. The experimental results show that the output voltage fluctuates within $\pm$ 6% of the rated voltage when the output power changes from 10 to 30 W. The BER is only about 0.3% under various operating conditions, which indicates that there is no bad interference between power transmission and bidirectional data transmission. The feasibility and effectiveness of the proposed full-duplex SWPDT system are verified. The main defect of this technology is that voltage stabilization is achieved by the circuit structure, and there is a small fluctuation in the output voltage when the load changes. Therefore, closed-loop control may be required to achieve better voltage stabilization.

REFERENCES

[1] Z. Yan, B. Song, Y. Zhang, K. Zhang, Z. Mao, and Y. Hu, "A rotation-free wireless power transfer system with stable output power and efficiency for autonomous underwater vehicles," *IEEE Trans. Power Electron.*, vol. 34, no. 5, pp. 4005–4008, May 2019.

[2] Y. Yao, S. Gao, Y. Wang, X. Liu, X. Zhang, and D. Xu, "Design and optimization of an electric vehicle wireless charging system using interleaved boost converter and flat solenoid coupler," *IEEE Trans. Power Electron.*, vol. 36, no. 4, pp. 3894–3908, Apr. 2021.

[3] J. H. Kim et al., "Development of 1-MW inductive power transfer system for a high-speed train," *IEEE Trans. Ind. Electron.*, vol. 62, no. 10, pp. 6242–6250, Oct. 2015.

[4] Z. Zhang and B. Zhang, "Omnidirectional and efficient wireless power transfer system for logistic robots," *IEEE Access*, vol. 8, pp. 13683–13693, 2020.

[5] R. Mai, Y. Liu, Y. Li, P. Yue, G. Cao, and Z. He, "An active-rectifier-based maximum efficiency tracking method using an additional measurement coil for wireless power transfer," *IEEE Trans. Power Electron.*, vol. 33, no. 1, pp. 716–728, Jan. 2018.

[6] X. Li, C. Tang, X. Dai, P. Deng, and Y. Su, "An inductive and capacitive combined parallel transmission of power and data for wireless power transfer systems," *IEEE Trans. Power Electron.*, vol. 33, no. 6, pp. 4980–4991, Jun. 2018.

[7] Y. Yao, P. Sun, X. Liu, Y. Wang, and D. Xu, "Simultaneous wireless power and data transfer: A comprehensive review," *IEEE Trans. Power Electron.*, vol. 37, no. 3, pp. 3650–3667, Mar. 2022.

[8] T. Wang, Q. Xu, W. Jia, Z.-H. Mao, H. Tang, and M. Sun, "Dual-functional wireless power transfer and data communication design for micromedical implants," *IEEE Trans. Emerg. Sel. Topics Power Electron.*, vol. 9, no. 5, pp. 6259–6271, Oct. 2021.

[9] Z. Y. an, Z. Xiang, L. Wu, and B. Wang, "Study of wireless power and information transmission technology based on the triangular current waveform," *IEEE Trans. Power Electron.*, vol. 33, no. 2, pp. 1368–1377, Feb. 2018.

[10] Y. Yao et al., "Analysis and design of a simultaneous wireless power and data transfer system featuring high data rate and signal-to-noise ratio," *IEEE Trans. Ind. Electron.*, vol. 68, no. 11, pp. 10761–10771, Nov. 2021.

[11] G. Wei, J. Feng, J. Zhang, C. Wang, C. Zhu, and S. Y. Ostanin, "An efficient power and data synchronous transfer method for wireless power transfer system using double-D coupling coil," *IEEE Trans. Ind. Electron.*, vol. 68, no. 11, pp. 10643–10653, Nov. 2021.

[12] L. Yang et al., "Undersea wireless power and data transfer system with shared channel powered by marine renewable energy system," *IEEE Trans. Emerg. Sel. Topics Circuits Syst.*, vol. 12, no. 1, pp. 242–250, Mar. 2022.

[13] L. Ji, L. Wang, C. Liao, and S. Li, "Simultaneous wireless power and bidirectional information transmission with a single-coil, dual-resonant structure," *IEEE Trans. Ind. Electron.*, vol. 66, no. 5, pp. 4013–4022, May 2019.

[14] Y. Sun, P. X. Yan, Z. H. Wang, and Y. Y. Luan, "The parallel transmission of power and data with the shared channel for an inductive power transfer system," *IEEE Trans. Power Electron.*, vol. 31, no. 8, pp. 5495–5502, Aug. 2016.

[15] Y. Yao, H. Cheng, Y. Wang, J. Mai, K. Lu, and D. Xu, "An FDM-based simultaneous wireless power and data transfer system functioning with high-rate full-duplex communication," *IEEE Trans. Ind. Inform.*, vol. 16, no. 10, pp. 6370–6381, Oct. 2020.

[16] P. Wang, Y. Sun, T. Feng, Y. Fan, and Y. Feng, "Simultaneous wireless power and data transfer system with full-duplex mode based on double-side LCCL and dual-notch filter," *IEEE Trans. Emerg. Sel. Topics Power Electron.*, vol. 10, no. 3, pp. 3140–3151, Jun. 2022.

[17] Z. Qian, R. Yan, J. Wu, and X. He, "Full-duplex high-speed simultaneous communication technology for wireless EV charging," *IEEE Trans. Power Electron.*, vol. 34, no. 10, pp. 9369–9373, Oct. 2019.

[18] Y. Fan, Y. Sun, X. Dai, Z. Zuo, and A. You, "Simultaneous wireless power transfer and full-duplex communication with a single coupling interface," *IEEE Trans. Power Electron.*, vol. 36, no. 6, pp. 6313–6322, Jun. 2021.

[19] P. Wang, Y. Sun, Y. Feng, T. Feng, Y. Fan, and X. Li, "An improvement of SNR for simultaneous wireless power and data transfer system with full-duplex communication mode," *IEEE Trans. Power Electron.*, vol. 37, no. 2, pp. 2413–2424, Feb. 2022.

[20] Y. Yao, Y. Wang, X. Liu, H. Cheng, M. Liu, and D. Xu, "Analysis, design, and implementation of a wireless power and data transmission system using capacitive coupling and double-sided LCC compensation topology," *IEEE Trans. Ind. Appl.*, vol. 55, no. 1, pp. 541–551, Jan./Feb. 2019.

[21] A. Trigui et al., "Generic wireless power transfer and data communication system based on a novel modulation technique," *IEEE Trans. Circuits Syst. I, Reg. Papers*, vol. 67, no. 11, pp. 3978–3990, Nov. 2020.

Yongzhi Jing received the M.S. and Ph.D. degrees in electrical engineering from Southwest Jiaotong University, Chengdu, China, in 2005 and 2014, respectively.

He is currently an Associate Research Fellow with the Department of Electrical Engineering, Southwest Jiaotong University. His main research interests include wireless power transfer, power electronics technology, maglev train, and maglev technology.

Wei Feng received the B.S. degree in electrical engineering from Hubei University of Technology, Wuhan, China, in 2020. He is currently working toward the M.S. degree in power electronics with the Department of Electrical Engineering from Southwest Jiaotong University.

His main research interests include wireless power transfer and power electronics technology.

Ke Qiao received the B.S. degree in electrical engineering in 2021 from Southwest Jiaotong University, Chengdu, China, where he is currently working toward the M.S. degree in power electronics with the Department of Electrical Engineering.

His current research interests include wireless power transfer and power electronics technology.

Liangtao Yang received the B.S. degree in measurement and control technology and instrumentation from Chengdu University of Technology, Chengdu, China, in 2021. He is currently working toward the M.S. degree in power electronics with the Tangshan Graduate School, Southwest Jiaotong University, Chengdu, China.

His main research interests include wireless power transfer and power electronics technology.

Sen Wang received the B.S. degree in electronic information science and technology in 2019 from Southwest Jiaotong University, Chengdu, China, where he is currently working toward the M.S. degree in power electronics with the Department of Electrical Engineering.

His current research interests include sensorless levitation system technology and wireless energy transfer.

Linhai Lu received the B.S. degree in electrical engineering from Xi'an University of Technology, Xi'an, China, in 2020. He is currently working toward the M.S. degree in power electronics with the Tangshan Graduate School, Southwest Jiaotong University.

His main research interests include wireless power transfer and power electronics technology.